Acknowledgement

This paper is published by ASCE
Journal of Structural Engineering, 2023,

Vol 149, issue 4 - April 2023

https://doi.org/10.1061/JSENDH.STENG-11779

An Adaptive Section Discretization Scheme for the Nonlinear Dynamic Analysis of Steel Frames

Svetlana M. Kostic[1] and Filip C. Filippou[2]

[1]Ph.D., University of Belgrade Faculty of Civil Engineering, Bulevar kralja Aleksandra 73, 11000 Belgrade, Serbia. Email: svetlana@grf.bg.ac.rs (corresponding author)

[2]Professor, Department of Civil and Environmental Engineering, University of California, Berkeley, CA 94720-1710. Email: filippou@berkeley.edu

ABSTRACT

The paper presents an adaptive section discretization scheme for the inelastic response analysis of structural members with cross sections that can be decomposed into rectangular and circular subdomains. Each subdomain can consist of a different material. As long as the largest strain in a subdomain does not exceed the specified trigger strain values, the subdomain contribution to the section response is determined by the numerically exact cubature rule for the subdomain. Once the largest strain reaches the trigger value for a subdomain, it is discretized with a fiber mesh and the numerical evaluation of its contribution to the section response is determined with the midpoint integration rule. The fiber mesh with the midpoint integration rule remains in effect for the activated subdomain until the end of the response history. The paper applies the adaptive discretization scheme to the thin-walled sections common in metallic structures and investigates the effect of different trigger strain values on the accuracy and computational efficiency of the inelastic response analysis of wide-flange steel sections and multi-story steel frames under static and dynamic excitations.

INTRODUCTION

Nonlinear static and dynamic analyses are commonly used in the evaluation of new and existing structures under performance-based engineering requirements. In this context, the numerical model of the structure needs to be robust, accurate, and computationally efficient. Among the different models developed in the past, nonlinear fiber beam/column elements are widely used for the simulation of the inelastic response of moment resisting frames, because they balance accuracy with computational efficiency, as several studies on the simulation of RC, steel, and composite steel-concrete frames have demonstrated (Kostic and Filippou 2012; Terzic and Stojadinovic 2015; Hajjar et al. 1998; Minafò and Camarda 2021; Cheng and Shing 2022).

In the formulation of a fiber-based beam/column element, the inelastic deformations are monitored at two or more cross sections along the element length (Neuenhofer and Filippou 1997; Scott et al. 2008). These cross sections are discretized into a number of integration points or fibers, so that the evaluation of the section response can be performed numerically. Consequently, the numerical accuracy and computational efficiency of the section evaluation depend on the integration rule and the number of integration points for the discretization. With increasing number of integration points the numerical accuracy increases with an almost proportional increase in computation time. It is, therefore, important to select the optimal number of integration points for optimizing the speed of computation without undue sacrifice in accuracy.

To date, few studies have addressed the optimisation of the fiber cross section integration. Because of its effect on the computation time, this issue is important for the seismic response analysis under a large suite of ground motions, as is currently the case in professional practice for the dynamic response analysis of structures in regions of high seismic risk. It is also of importance in system identification studies that require numerous analyses with different input parameters. Berry and Eberhard (2008) made a proposal for the efficient discretization of circular reinforced concrete sections. Kostic and Filippou (2012) analyzed various integration rules for the section discretization problem. They concluded that the higher-order integration rules do not offer gains over the midpoint integration rule under inelastic deformations. In addition, they made practical recommendations for the discretization of steel wide flange sections and rectangular reinforced concrete sections. Quagliaroli et al. (2015) proposed a subdomain discretization in combination with Gauss quadrature rules for the accurate determination of the ultimate strength of

RC sections. None of these studies, however, study the problem under the aspect of an adaptive section discretization.

A couple of recent studies investigated adaptive section discretization strategies. Guided by the insight that only a small percentage of the sections experience inelastic deformations during the nonlinear analysis of the structural model, while the majority remain in the linear elastic range, He and co-workers proposed an analysis strategy that starts with all sections in the linear elastic range (He et al. 2017a; He et al. 2017b) and replaces the discretization of sections that exceed prescribed strain limits by a standard fiber mesh. More recently, Kostic and Filippou (2022) proposed a more general adaptive section discretization scheme for rectangular and circular cross sections for RC and composite steel-concrete structural members. The proposal divides each section into circular or rectangular concentric "rings". As the section deformations increase, the rings with inelastic strains above specified limits are discretized with a standard fiber mesh, while the inner portion of the section that remains in the linear elastic range uses exact cubature rules for the determination of its contribution to the section forces and stiffness. The computational time savings range from 30% to 75% without affecting the accuracy of the response. This method is, however, limited to solid circular and rectangular sections that allow the subdivision of the integration domain into concentric circular or rectangular "rings". For sections with complex geometries that do not meet this subdivision criterion, as is the case for the wide-flange (WF) profiles of metallic structural members, a more general subdivision scheme of the integration domain is required.

The general domain subdivision method in this paper extends the idea of section subdivision with gradual activation of a subdomain to sections of arbitrary shape composed of circular or rectangular subdomains. Because each subdomain may be assigned a different material model, the proposed adaptive scheme applies to homogeneous as well as to non-homogeneous sections. The method uses the exact cubature rule for a circular or rectangular subdomain before the trigger strains are exceeded and replaces the cubature rule with a standard mesh discretization of the subdomain thereafter. The proposed adaptive discretization scheme is implemented at the section level, so that it can be used with any type of fiber beam-column element following the organization for the element state determination in Scott et al. (2008). The paper demonstrates the computational benefits of the proposed scheme for metallic structures with thin-walled cross sections.

ADAPTIVE SECTION DISCRETIZATION FOR THIN-WALLED SECTIONS

The determination of the stress resultants $\mathbf{s}$ and the section stiffness matrix $\mathbf{k_s}$ for a beam/column element with plane sections remaining plane after deformation involves the following integrals over the section area A

$$\mathbf{k_s} = \int_A E_t \begin{bmatrix} 1 & -y & z \\ -y & y^2 & -yz \\ z & -yz & z^2 \end{bmatrix} dA \tag{1}$$

$$\mathbf{s} = \begin{pmatrix} N \\ M_z \\ M_y \end{pmatrix} = \int_A \begin{pmatrix} 1 \\ -y \\ z \end{pmatrix} \sigma\, dA \tag{2}$$

where E_t is the tangent modulus and σ the normal stress at the material point with coordinates (y, z) relative to the section coordinate system. N is the normal force and M_y, M_z are the bending moments about the axes y and z, respectively. The numerical evaluation of these integrals over the cross section area A gives:

$$\mathbf{k_s} \approx \sum_{i=1}^{nf} E_{ti} \begin{bmatrix} 1 & -y_i & z_i \\ -y_i & y_i^2 & -y_i z_i \\ z_i & -y_i z_i & z_i^2 \end{bmatrix} A_i \tag{3}$$

$$\mathbf{s} \approx \sum_{i=1}^{nf} \begin{pmatrix} 1 \\ -y_i \\ z_i \end{pmatrix} \sigma_i A_i \tag{4}$$

where nf is the number of integration points (IPs) or fibers. The subscript i refers to the variables of the i-th fiber with A_i playing the role of an integration weight that for the midpoint integration rule can be visualized as the fiber area. When the modulus of elasticity E_t is constant over the area A, as is the case under linear elastic conditions, the integrals in Eqs. (1)-(2) involve at most quadratic polynomials in y and z.

The exact evaluation of integrals involving polynomials over a circular or rectangular domain uses cubature formulas with a small number of integration points (IPs) (Abramowitz et al. 1964; Cools 2003). Fig. 1 shows the cubature rule for the unit square area with the integration points located at $(\pm\frac{\sqrt{3}}{3}, \pm\frac{\sqrt{3}}{3})$ with weights equal to $\frac{1}{4}$.

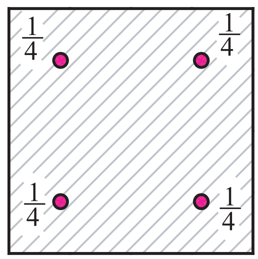

Fig. 1. Cubature rule for a unit square area with 4 IPs.

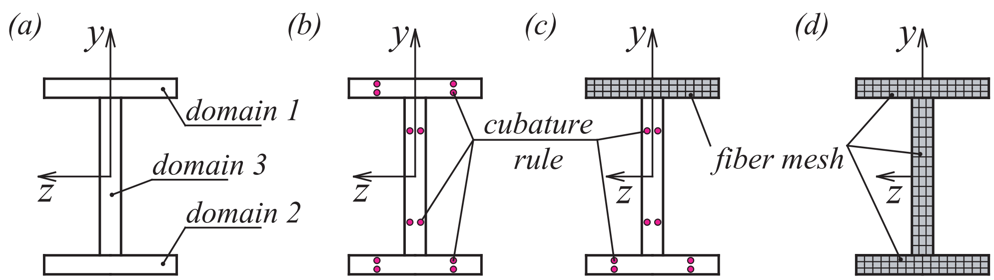

Fig. 2. Adaptive section discretization scheme for wide flange section: (a) division into 3 rectangular subdomains, (b) cubature rule for initial response, (c) fiber mesh for top flange after its activation, (d) section discretization after activation of all subdomains.

The proposed adaptive discretization scheme will be illustrated with the example of a thin-walled, wide-flange section in Fig. 2. Before the start of the inelastic response analysis the section is subdivided into a number of rectangular subdomains. The simplest choice subdivides the section into three rectangular domains, as Fig. 2(a) shows: one for the upper flange (domain 1), one for the lower flange (domain 2), and one for the web (domain 3). The input data also include the fiber mesh parameters for the numerical evaluation of the contribution of each subdomain to the section

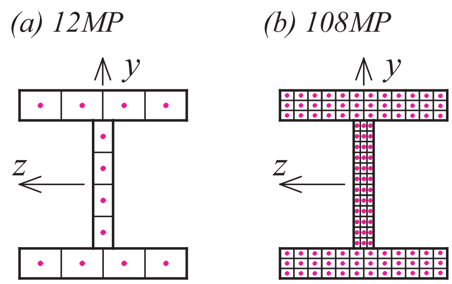

Fig. 3. Recommendations for wide flange section discretization with the midpoint integration rule from Kostic and Filippou (2012): (a) 12 MP scheme, (b) 108 MP scheme.

integrals once the trigger strains are exceeded during the response history. The fiber mesh selection depends on the target accuracy for the inelastic response. Fig. 3(a) shows the coarsest recommended mesh from the study by Kostic and Filippou (2012) involving 4 midpoint integration points in each flange and in the web in the arrangement 1x4 for a total of 12. It is denoted with 12MP. Fig. 3(b) shows the finest recommended mesh from the study by Kostic and Filippou (2012) involving 36 midpoint integration points in each flange and in the web in the arrangement 3x12 for a total of 108 integration points. It is denoted with 108MP. Finally, the input data also include the positive and negative trigger strain values ε_{lim^+} and ε_{lim^-}, respectively, for each subdomain. These values are equal to the yield strain of the metallic material or a small multiple of it, as will be discussed in the evaluation studies of the next sections. For non-homogeneous sections the specified trigger strains may vary from one subdomain to the next.

With this input information, the inelastic response analysis can commence. At the start of the analysis, each rectangular subdomain of the wide-flange section in Fig. 2(a) uses the cubature rule in Fig. 1 with 4 IPs, as Fig. 2(b) shows. When the largest normal strain at one of the corners of a rectangular subdomain exceeds the trigger value, the subdomain integration changes from the cubature rule to a fiber mesh with the midpoint integration rule, as is the case for the flange in Fig. 2(c). The switch from the cubature rule to the fiber mesh with midpoint integration rule is called "subdomain activation" in this paper. Once the fiber mesh comes into effect for a subdomain, it remains in effect until the conclusion of the inelastic response history. Fig. 2(d) shows the discretization of the cross section for the case that both flanges and the web are activated at some point of the response history. The fiber mesh for each rectangular subdomain in Fig. 2(c) and (d) uses the finest recommended discretization of 3x12 from the study by Kostic and Filippou (2012). It is possible to subdivide the wide-flange section into more rectangular subdomains, but the gains may be offset by the computational overhead for checking the trigger strain values in each subdomain.

It is also possible to use a coarser fiber mesh discretization for the adaptive scheme. The study by Kostic and Filippou (2012) recommends a fiber mesh with 2x8 IPs in the flanges and 8x1 IPs in the web for a total of 40 IPs, if the axial strains are of secondary interest in the columns. Instead the coarse mesh alternative of 1x4 IPs for each subdomain is not recommended for the adaptive scheme, because it has accuracy limitations under biaxial flexure while offering significantly smaller computational savings relative to the non-adaptive scheme with the same mesh discretization. This issue will be discussed further in the context of the inelastic response analysis of a 6-story steel frame under bidirectional ground excitation.

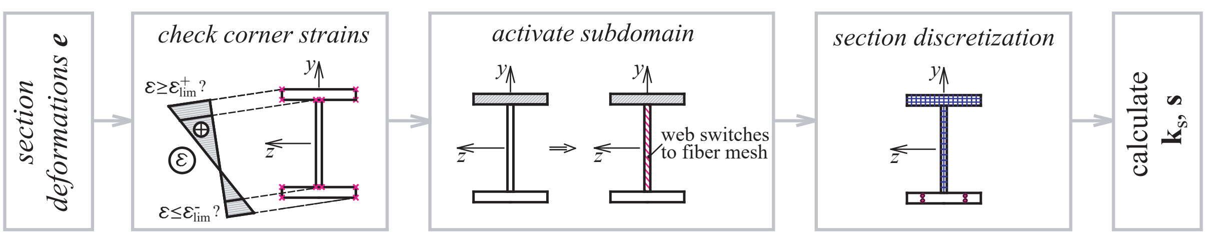

Fig. 4. Schematic outline of adaptive section discretization for a wide-flange section.

Fig. 4 shows a schematic outline of the adaptive section discretization. For given section deformations **e** the normal strains at the corners of each rectangular subdomain are compared with the trigger strain values. If the largest normal strain exceeds the trigger strain, the corresponding subdomain is "activated" by changing the numerical evaluation of its contribution to the section resultants and the section stiffness matrix from the cubature rule to the 3x12 fiber mesh with the midpoint integration rule, as is the case for the web in the middle of Fig. 4. Once a subdomain is "activated", the fiber mesh with the midpoint integration rule remains in effect for the remainder of the analysis, as is the case for the flange in the middle of Fig. 4. The computational savings are rather significant for cases involving the activation of a few section subdomains in a large structural model.

NUMERICAL SIMULATIONS

This section assesses the computational savings of the proposed adaptive section discretization for the inelastic response of sections under large inelastic strain reversals and for the static and dynamic response of structural models under lateral loads inducing significant inelastic deformations. The computational savings are contrasted with the accuracy for the global and the local response for different trigger strain values for a section subdomain. The analytical studies were conducted with FEDEASLab, a Matlab-based general purpose framework for the nonlinear response analysis of structures (Filippou and Constantinides 2004).

Section analyses

The following section analyses demonstrate the relation between the response accuracy for the proposed adaptive section discretization and the selected trigger strain values $[\,\varepsilon_{lim^-}\,,\,\varepsilon_{lim^+}\,]$. For a material with a well defined yield strain and equal yield strength in tension and compression, it is reasonable to select as target strains $e_{lim,1} = [\,-\frac{f_y}{E}\,,\,\frac{f_y}{E}\,]$, where f_y is the yield strength and E is the elastic modulus of the material. With this selection the adaptive discretization achieves the same accuracy as the non-adaptive discretization with the same fiber mesh parameters for each subdomain. Delaying the subdomain activation with the selection of larger trigger strain values leads to slightly larger computational benefits of the adaptive discretization without undue penalty for the response accuracy. The following study uses the inelastic response of a W14x120 steel section to explore the response accuracy for two cases of larger trigger strain values: (a) a trigger strain of twice the yield strain $e_{lim,2} = [\,-2\frac{f_y}{E}\,,\,2\frac{f_y}{E}\,]$, and (b) a trigger strain of three times the yield strain $e_{lim,3} = [\,-3\frac{f_y}{E}\,,\,3\frac{f_y}{E}\,]$.

Among the load histories investigated in the study by Kostic and Filippou (2012) two challenging cases are selected:

1. Fig. 5(a) shows the first load history: two curvature cycles about the weak y-axis with

variable axial force simulating the effect of overturning moments. The curvature reversal value κ_y is equal to $3\kappa_{py}$ for the first cycle and equal to $6\kappa_{py}$ for the second, where κ_{py} is the curvature under the plastic moment capacity M_{py}. The axial force varies about the gravity compression value of $(-0.20)N_p$ with an amplitude of $(0.10)N_p$ for the first curvature cycle and $(0.20)N_p$ for the second, where N_p is the plastic axial capacity.

2. Fig. 5(b) shows the second load history: two biaxial curvature cycles under a constant axial compression of -20% N_p. The curvature κ_y about the weak axis is 10 times larger than the curvature κ_z about the strong axis. The curvature reversal value κ_z is equal to κ_{pz} for the first cycle and equal to $2\kappa_{pz}$ for the second, where κ_{pz} is the curvature under the plastic moment capacity M_{pz}.

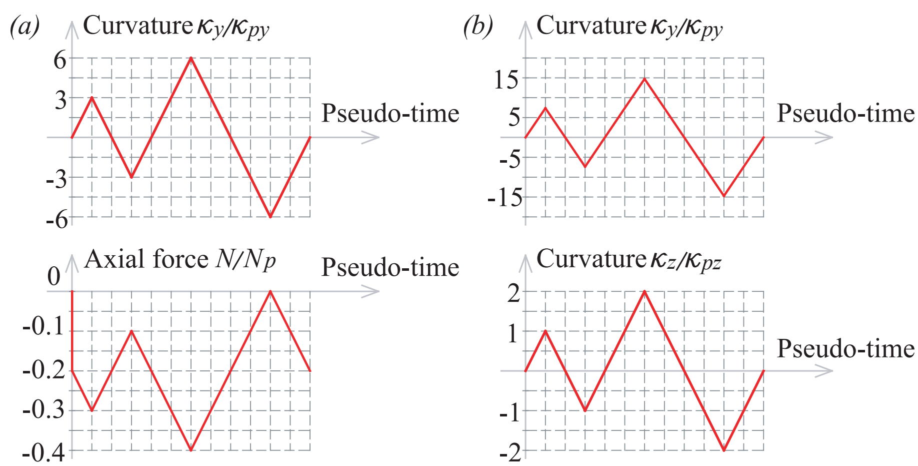

Fig. 5. Load history for section analyses: (a) curvature about y-axis with variable axial force, and (b) biaxial curvature under constant axial force $N = (-0.20)N_p$

.

Figs. 6 and 7 show the response history of the W14x120 steel section for the first load history. The results are presented for two non-adaptive and three adaptive section discretizations with different trigger strain values. The non-adaptive fiber mesh discretizations correspond to the fine mesh of 108 IPs in 3(b), representing the reference solution, and the coarse mesh of 12 IPs in 3(a), denoted with 12MP in the figures. Both non-adaptive discretizations use the midpoint integration rule. The adaptive section discretizations use one rectangular subdomain for each flange and the web. Once activated, a subdomain uses a fiber mesh of 3x12, as shown in Fig. 2, with the midpoint integration rule. The three adaptive discretization cases correspond to trigger strain values of $e_{lim,1}$, $e_{lim,2}$ and $e_{lim,3}$ for the activation of a subdomain.

The uniaxial material modal for the homogeneous section is based on J2 plasticity with kinematic and isotropic hardening Simo and Hughes (1998). The following results are independent of the specified yield strength f_y = 470 MPa and elastic modulus E = 200 GPa, because the loading and the response variables are normalized with respect to the plastic capacities and the corresponding deformations. The kinematic and isotropic hardening modulus of the material is set equal to a very small value for numerical stability purposes.

The results of the reference solution in Figs. 6 and 7 are numerically exact for all practical purposes Kostic and Filippou (2012). The adaptive discretization with trigger strain values $e_{lim,1}$ equal to the yield strain of the material produces identical results with the reference solution in Fig. 6(a) and Fig. 7(a). This happens because the cubature rule is exact for the contribution of each rectangular subdomain to the section response before its activation, and the fiber mesh of the subdomain is the same as for the reference solution after its activation. The results are also excellent for the adaptive discretization $e_{lim,2}$ with trigger strain values of twice the yield strain, both in terms of the moment-curvature history in Fig. 6(b) and the normal force-axial strain history in Fig. 7(b) except for a slight discrepancy for the delayed transition from the linear elastic to the inelastic response. The results for the adaptive discretization $e_{lim,3}$ with trigger strain values of three times the yield strain show a bigger discrepancy for the delayed transition from the linear elastic to the inelastic response Figs. 6(b) and 7(b), but are still in good agreement with the reference solution for the remainder of the moment-curvature history in Fig. 6(b). A slight error remains, however, for the normal force-axial strain history in Fig. 7(b), which increases with increasing axial deformation. In contrast to the excellent results of the three adaptive discretization schemes, the accuracy limitations of the section discretization with a coarse fiber mesh are evident for the moment-curvature history in Fig. 6(a), but especially for the normal force-axial strain history in Fig. 7(a).

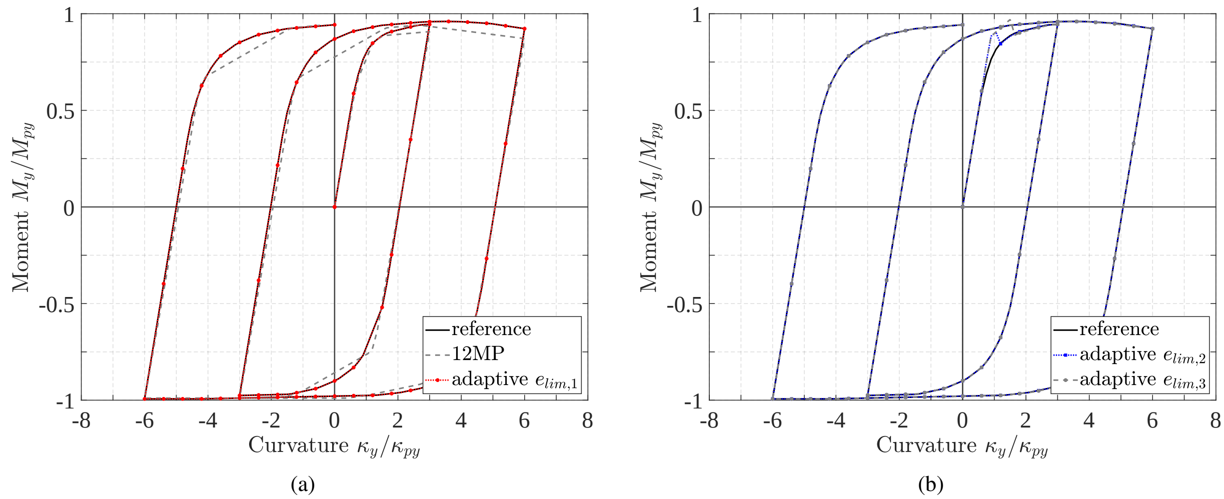

Fig. 6. Moment-curvature history for W14x120 steel section under variable axial force for two-non adaptive and 3 adaptive discretizations with strain limits $e_{lim,1}$, $e_{lim,2}$ and $e_{lim,3}$.

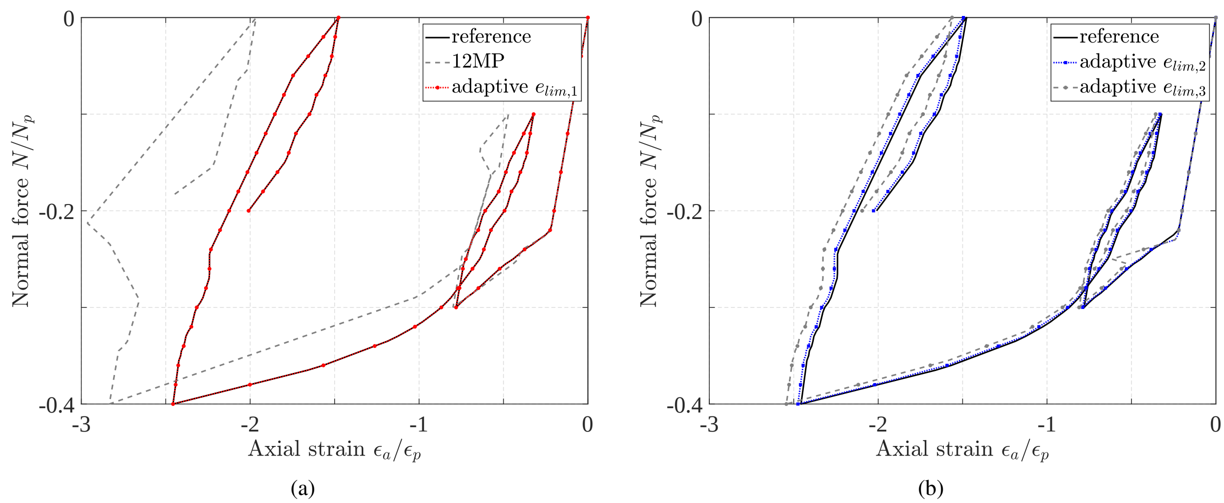

Fig. 7. Axial force-axial strain history for W14x120 steel section under variable axial force for two-non adaptive and 3 adaptive discretizations with strain limits $e_{lim,1}$, $e_{lim,2}$ and $e_{lim,3}$.

The second load history with biaxial flexural deformations under dominant bending about the weak $y-$axis of the wide flange section was selected because it is the most challenging from the standpoint of response accuracy (Kostic and Filippou 2012).

Figs. 8 - 10 show the moment-curvature history about the two principal axes and the normal force-axial strain history for the W14x120 section with bilinear material. The results of the reference solution in Figs. 8 - 10 are numerically exact for all practical purposes Kostic and Filippou (2012).

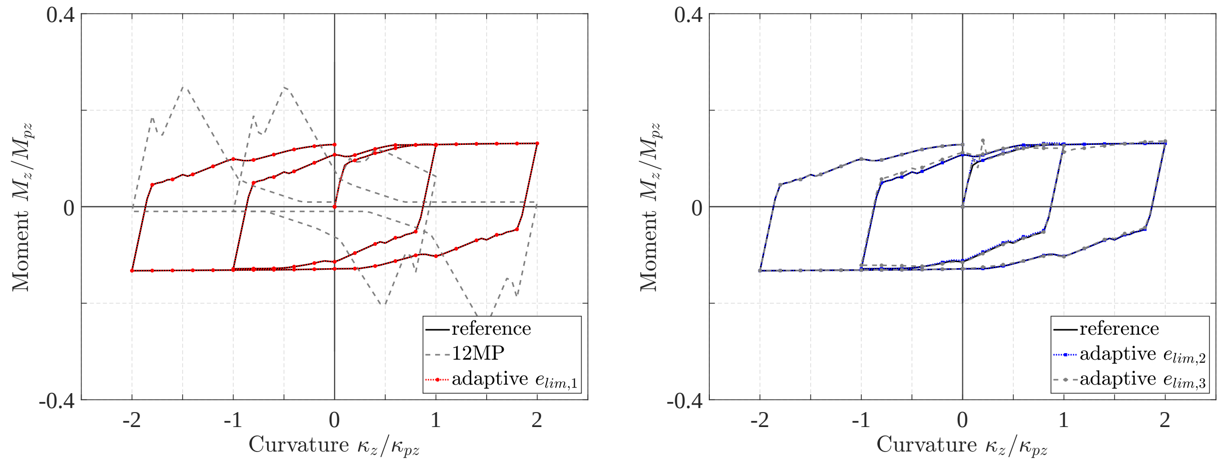

(a) (b)

Fig. 8. Moment-curvature history about the z-axis for W14x120 steel section under constant axial force for two-non adaptive and 3 adaptive discretizations with strain limits $e_{lim,1}$, $e_{lim,2}$ and $e_{lim,3}$.

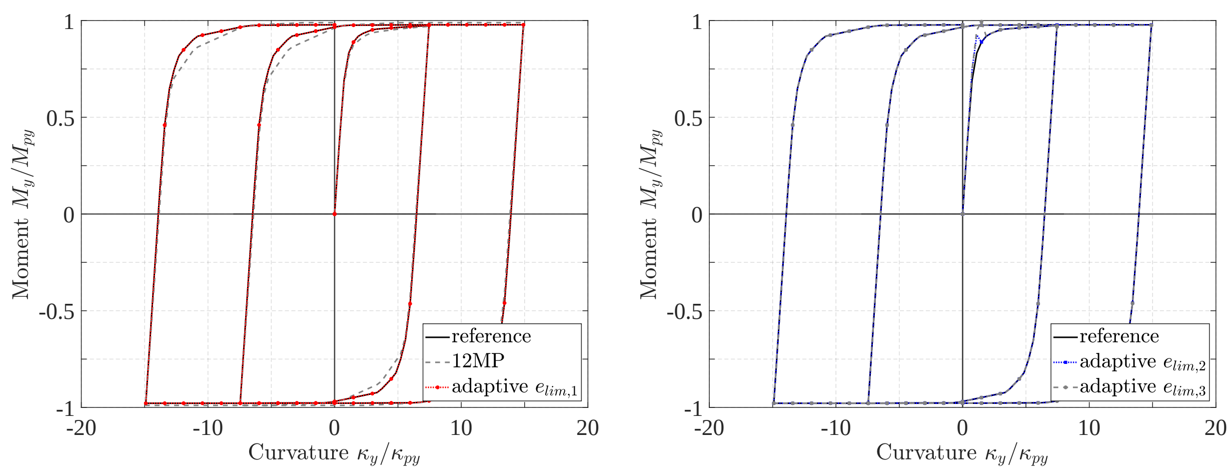

(a) (b)

Fig. 9. Moment-curvature history about the y-axis for W14x120 steel section under constant axial force for two-non adaptive and 3 adaptive discretizations with strain limits $e_{lim,1}$, $e_{lim,2}$ and $e_{lim,3}$.

The adaptive discretization with trigger strain values $e_{lim,1}$ equal to the yield strain of the material produces again identical results with the reference solution in Figs. 8(a), 9(a) and 10(a). The results are also excellent for the adaptive discretization $e_{lim,2}$ with trigger strain values of twice the yield strain in Figs. 8(b), 9(b) and 10(b). In fact, except for a slight discrepancy for the delayed transition from the linear elastic to the inelastic response these results are practically indistinguishable from the reference solution. The results for the adaptive discretization $e_{lim,3}$ with trigger strain values of

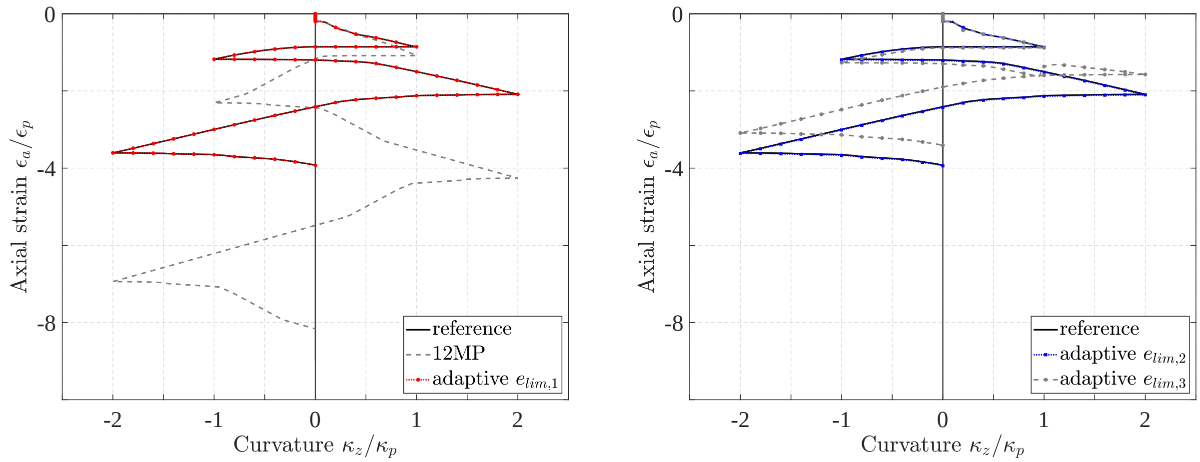

(a) (b)

Fig. 10. Axial force-axial strain history for W14x120 steel section under constant axial force for two-non adaptive and 3 adaptive discretizations with strain limits $e_{lim,1}$, $e_{lim,2}$ and $e_{lim,3}$.

three times the yield strain also show very good agreement with the reference solution in Figs. 8(b), 9(b) and 10(b) except for the slightly more pronounced discrepancy for the delayed transition from the linear elastic to the inelastic response for the moment-curvature history and the slight underestimation of the axial strain in Fig. 10(b) with maximum error of about 15%. Such error may still be acceptable for the inelastic response analysis of a multi-story steel frame, as will be discussed later. In contrast to the excellent results of the three adaptive discretization schemes, the accuracy limitations of the section discretization with a coarse fiber mesh are evident for the normal force-axial strain history in Fig. 10(a), but especially for the moment-curvature history about the strong z-axis of the wide flange section in Fig. 8(a). Such a coarse fiber mesh discretization is unsuitable for this type of biaxial flexural deformation response, as already pointed out by Kostic and Filippou (2012).

For the computational savings of the three adaptive discretization schemes it is relevant to consider the activation results in Table 1. Noting that the total number of load steps for both load histories is 261, it is clear that modest computational savings result from the late activation of the web for the uniaxial load history under trigger strain values $e_{lim,1}$ and $e_{lim,2}$. Without web activation, the computational savings are slightly larger for the trigger strain values $e_{lim,3}$. The computational savings are minimal for the biaxial load history with trigger strain values $e_{lim,1}$ and $e_{lim,2}$ and modest with trigger strain values $e_{lim,3}$ that do not lead to web activation. It is worth mentioning, however, that the early excursion into the inelastic range for both load histories is rather unfavorable to the adaptive discretization scheme. The conclusion about computational savings would be quite different for load histories with several early cycles under small inelastic excursions. This is the case for many sections of structural models, as will be demonstrated in the next section.

TABLE 1. Load steps for subdomain activation during section analyses.

Trigger strains	Uniaxial load history			Biaxial load history		
	flange 1	flange 2	web	flange 1	flange 2	web
$e_{lim,1}$	25	25	120	23	23	28
$e_{lim,2}$	29	29	134	24	25	41
$e_{lim,3}$	32	32	–	28	29	–

In conclusion, the section analyses show that the adaptive discretization with trigger strain values of $e_{lim,1}$ and $e_{lim,2}$ produces results that are practically identical with the reference solution with a non-adaptive fiber mesh of 108 integration points. For a single section the computational benefits of these adaptive discretizations are modest, especially under a load history with an early excursion into large inelastic deformations. Because the computational benefit is more appreciable for the adaptive discretization with trigger strain values $e_{lim,3}$ while the error remains relatively small, it is retained for further investigation of its global and local response accuracy for the multi-story frames in the next section, for which the computational savings from the adaptive section discretization strategy promise to be appreciable.

Multi-story steel frames

This section investigates the accuracy and the computational benefits of the proposed adaptive discretization scheme for the inelastic response analysis of a 20-story frame under static loads and of a 6-story frame under bidirectional ground accelerations.

The numerical model for both frames uses a force-based, fiber beam-column element for each member with a 4-point Gauss-Lobatto rule for the numerical integration along the element axis

(Taucer et al. 1991). At each integration point the numerical evaluation of the section response uses either a fiber mesh with 108 IPs for the reference solution, or an adaptive discretization with a rectangular subdomain for each flange and the web. Each subdomain uses the exact cubature rule before activation, and switches to a 3x12 fiber mesh once activated when the largest normal strain exceeds the specified trigger value, as discussed in connection with Figs. 2 and 4. The inelastic response analysis of both frames accounts for nonlinear geometry effects under large displacements with the corotational formulation (Crisfield 1996).

Pushover analysis of twenty story steel frame

The inelastic response analysis under static loads concerns the 20-story space frame in Fig. 11 from the original study by Orbison et al. (1982) and several subsequent studies (Chiorean 2009; Ngo-Huu et al. 2007). The frame is subjected to concentrated nodal forces corresponding to gravity loads of 4.8 kN/m^2, and to a gradually increasing wind load of 0.96 kN/m^2 in the Y direction acting on the facade at $Y = 0$. Fig. 11 lists the wide flange profiles for the columns and the girders of the frame. The steel material has yield strength $f_y = 344.8$ MPa and elastic modulus $E = 200$ GPa. The uniaxial material model for the fiber-beam column elements is assumed to be linear elastic, perfectly plastic.

Fig. 12 shows the inelastic response of the 20-story frame in terms of the relation between the load factor for the lateral loading and the horizontal drift ratio in the Y-direction for point A on the roof of the building. The latter is expressed by the ratio of the horizontal translation U_{YA} for point A in the Y-direction and the total height H of the 20-story frame. The load-displacement response of the model for the reference solution with a fiber mesh of 108 IPs at each of 4 integration points of the fiber-beam column elements gives an ultimate load factor of 1.08 in very good agreement with the load factor 1.06 reported by Chiorean (2009).

Fig. 12(a) shows that the results of the adaptive section discretization with trigger strain values $e_{lim,1}$ equal to the yield strain are identical with the reference solution. In Fig. 12(b) the adaptive discretizations $e_{lim,2}$ and $e_{lim,3}$ with trigger strain values equal to twice or three times the yield strain, respectively, show a slightly larger ultimate load factor of 1.09 and 1.10, respectively. A

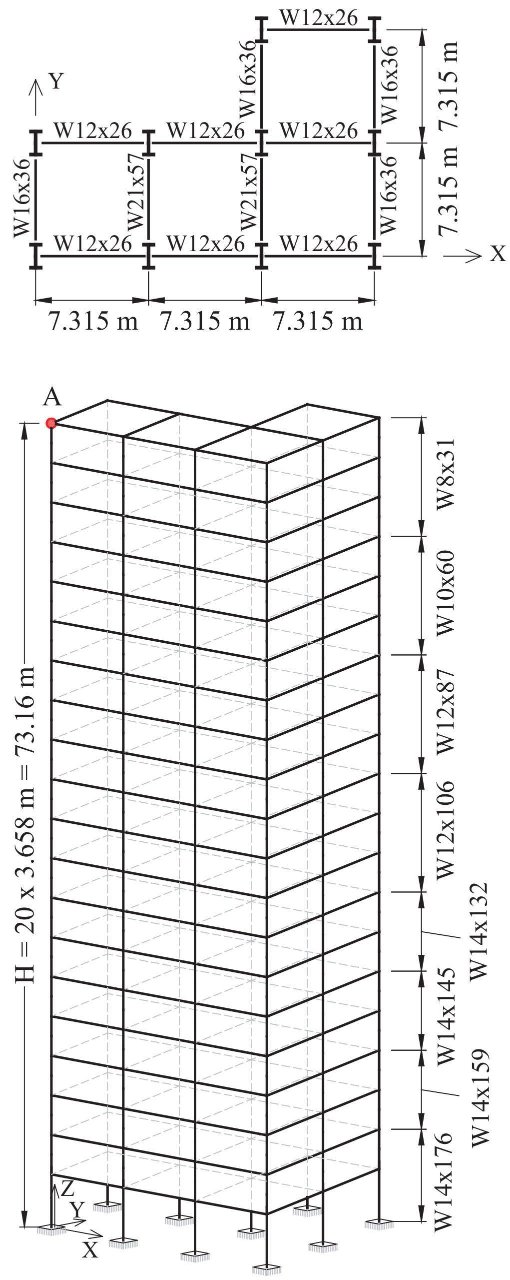

Fig. 11. Twenty-story frame

marker on the load-displacement relation for the adaptive section discretizations in Fig. 12(a) and (b) marks the load step at the first subdomain activation. The delay of the first subdomain activation for larger trigger strain values is evident from the comparison of the responses in Fig. 12(b) for the trigger strain values $e_{lim,2}$ and $e_{lim,3}$ with the response in Fig. 12(a) for trigger strain values $e_{lim,1}$. This delay has a small effect on the accuracy of the inelastic response and on the ultimate load

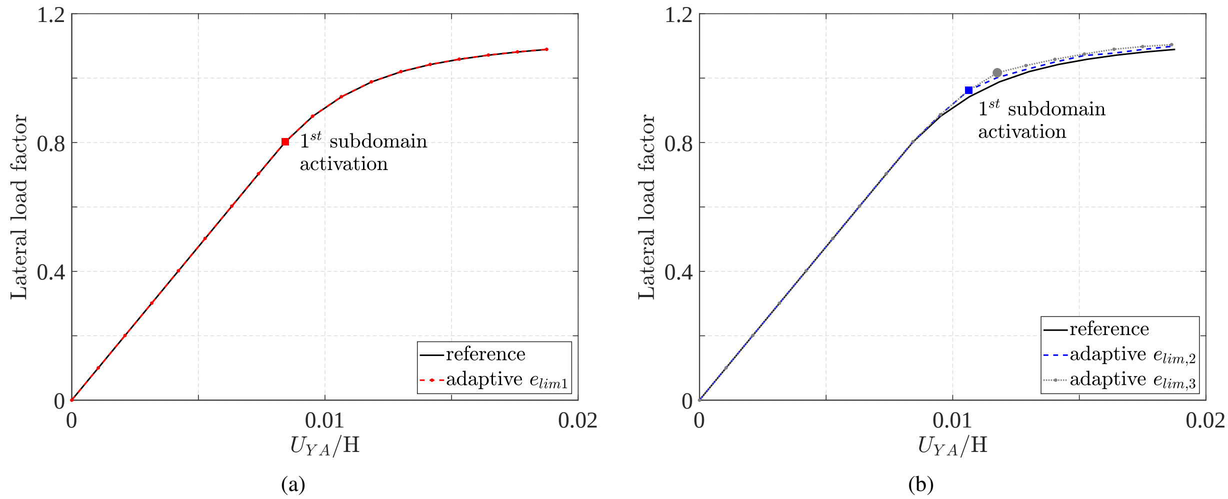

Fig. 12. Load-displacement response of 20-story frame for the non-adaptive section discretization with 108 MP and three adaptive schemes with strain limits $e_{lim,1}$, $e_{lim,2}$ and $e_{lim,3}$

factor value for the adaptive section discretization schemes in Fig. 12(b).

The smooth transition of the inelastic response relation during the activation of the first subdomain and all subsequent activations distinguishes the proposed adaptive section discretization scheme from an earlier proposal for an adaptive section activation (He et al. 2017a; He et al. 2017b).

TABLE 2. Relative computation time with number of fully and partially activated sections at the conclusion of the pushover analysis for the 20-story frame

Discretization	Time	No of fully activated sections	No of partially activated sections
Reference	100%	/	/
Adaptive $e_{lim,1}$	24%	67	77
Adaptive $e_{lim,2}$	22%	50	53
Adaptive $e_{lim,3}$	21%	36	38

Table 2 gives details about the computational effort for the adaptive section discretization schemes with trigger strain values $e_{lim,1}$, $e_{lim,2}$ and $e_{lim,3}$ relative to the reference solution with a non-adaptive fiber mesh of 108 IPs at each of 4 integration points of the fiber-beam column elements of the model. The table lists the number of fully and partially activated sections for the structural model at the end of the pushover analysis, and reports the computation time of each adaptive scheme relative to the time for the reference solution. The computation time is from 4.2 to

4.8 times shorter for the adaptive discretization schemes than for the reference solution depending on the selected trigger strain values.

The number of fully and partially activated sections should be compared with the total number of sections to be monitored in the model, which for 460 elements with 4 sections each amount to 1840. Even when one accounts for the fact that the two internal integration points of a beam-column element will not experience inelastic deformations for perfectly plastic material response in the absence of significant distributed element loads and reduces the number of sections to be monitored for inelastic action to 920, the cause for the computational savings is clear. Relaxing the trigger strain values from the yield strain ($e_{lim,1}$) to twice the yield strain ($e_{lim,2}$) reduces the number of fully and partially activated sections appreciably, but the savings in computation time are not worth the slight loss of accuracy. Similarly, the small additional savings from the relaxation of the trigger strain value to 3 times the yield strain do not justify the more appreciable loss of local response accuracy observed in the section response analyses.

In conclusion, the adaptive discretization schemes with trigger strain values of $e_{lim,1}$ and $e_{lim,2}$ offer comparable savings in computation time for the inelastic pushover analysis with a slight accuracy loss for the global and local inelastic response of the latter.

Dynamic response of six story frame under bidirectional ground acceleration

The inelastic response analysis under bidirectional ground accelerations concerns the irregular six-story frame in Fig. 13. The frame geometry is based on earlier studies by multiple authors (Chiorean 2009), but the structure underwent significant re-design to meet the current seismic design requirements of Eurocode 8 for a DCM ductility class. Fig. 13 shows the resulting column and girder sizes for the six-story frame noting that the columns of the six story block are oriented so that the strong axis of bending coincides with the global Y-axis, while the 6 columns of the 3-story portion have the strong axis of bending coincide with the global X-axis. The steel material has yield strength f_y = 250 MPa and elastic modulus E = 206.85 GPa. The uniaxial material model for the fiber-beam column elements is assumed to be linear elastic, perfectly plastic.

The gravity load of the frame amounts to 6 kN/m^2. It is used to set up the equivalent concentrated nodal forces due to gravity and in the determination of the lumped mass terms M_1 and M_2 in Fig. 13. The damping of the structural model is represented with the modal damping method of Wilson and Penzien with a 2% damping ratio for all modes. Four node linear elastic planar quadrilateral elements with high in-plane stiffness are used to constrain the motion of each floor to a translation in X, a translation in Y and a rotation about the Z-axis. The planar quadrilateral elements do not affect the translation in Z and the other rotations at each node, which are thus independent. The 6-story frame was subjected to the following ground acceleration records in both horizontal X- and Y-directions simultaneously with the name of the recording station in parentheses: Imperial Valley (Hotwille Post Office), Northridge (LA Hollywood Storage), Loma Prieta (Gilroy), Landers (Barstow), Kobe (Takatori), Kocaeli Turkey (Izmit), Chi-Chi Taiwan (CHY024) and Darfield, New Zealand (Page Road Pumping Station).

Because of the very small benefit in computation time for the case $e_{lim,3}$ in the nonlinear pushover analyses of the preceding section, the adaptive section discretization cases are limited to $e_{lim,1}$ with a trigger strain value equal to the yield strain, and $e_{lim,2}$ with a trigger strain value equal to twice the yield strain.

TABLE 3. Calculation time (in % of time for the reference solution) and error in the maximum value of the relative roof drift for the six-story frame under bidirectional earthquake loading.

Earthquake record	PGA	Adaptive $e_{lim,1}$ time	error	n_F/n_P	Adaptive $e_{lim,2}$ time	error	n_F/n_P
Imperial Valley-06	0.21g	29%	0.34%	11/45	21%	1.00%	0/5
Northridge-01	0.36g	39%	0.35%	37/95	25%	0.86%	14/25
Loma Prieta	0.36g	30%	0.15%	9/45	23%	0.24%	2/7
Landers	0.14g	22%	0.13%	0/5	20%	0.60%	0/0
Kobe	0.62g	51%	0.39%	79/121	39%	0.79%	51/67
Kocaeli Turkey	0.23g	27%	0.24%	5/39	21%	0.52%	0/2
Chi-Chi Taiwan	0.28g	33%	0.26%	22/59	25%	1.03%	7/17
Darfield N.Zealand	0.22g	28%	0.52%	15/45	23%	2.13%	2/10

Note: n_F - number of fully activated sections, n_P - number of partially activated sections.

Table 3 provides details about the computation time and the global response accuracy of the nonlinear response history analyses with the adaptive section discretization schemes with trigger strains $e_{lim,1}$ and $e_{lim,2}$ under the selected ground motions. The computation time is expressed

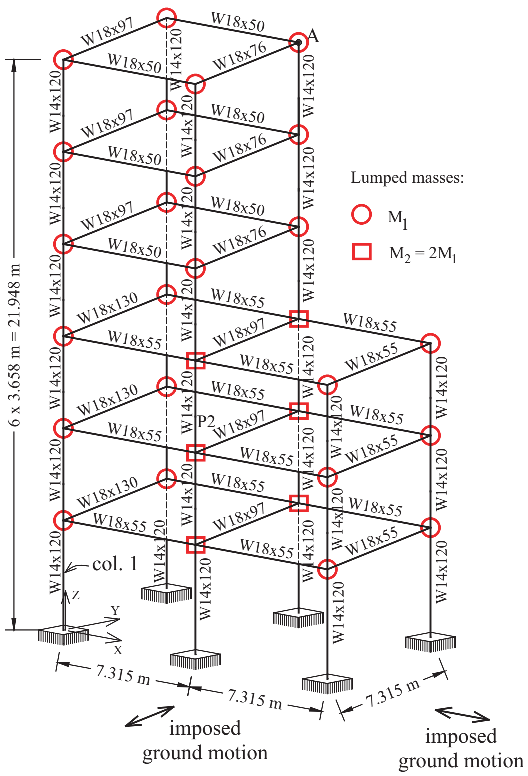

Fig. 13. Six-story frame

in % relative to the time for the reference solution with a non-adaptive discretization with a fiber mesh of 108 MP for each section. The table also lists the number n_F of fully activated sections and the number n_P of partially activated sections at the completion of the analysis. With 63 elements and 4 monitored sections for each element the total number of monitored sections for this model is 252. Because the integration points at the interior of each frame element remain elastic during the analysis, the maximum number of sections to be monitored for possible inelastic action is realistically half as many, i.e. 126. The table also lists the error in the maximum value for the relative lateral roof drift at point A in Fig. 13. The relative error is the difference between the maximum value for the reference solution and the maximum value for the adaptive section discretization normalized by the maximum value for the reference solution according to the following relation

$$error(\%) = \left| \frac{d_{max,reference} - d_{max,adaptive}}{d_{max,reference}} \right| \cdot 100 \tag{5}$$

The values in Table 3 show that the adaptive discretization $e_{lim,1}$ with a trigger strain value equal to the yield strain gives excellent results with a computation time from 2 to 4.5 times shorter than the reference solution depending on the ground motion. The largest error for the lateral roof drift value of the adaptive solution amounts to 0.52% of the reference solution. The largest error for the lateral roof drift value increases to 2.13% for the adaptive section discretization $e_{lim,2}$ with trigger strain values equal to twice the yield strain. The savings in computation time for the adaptive solution also increase with reductions from 2.6 to 5 times of the time for the reference solution depending on the ground motion.

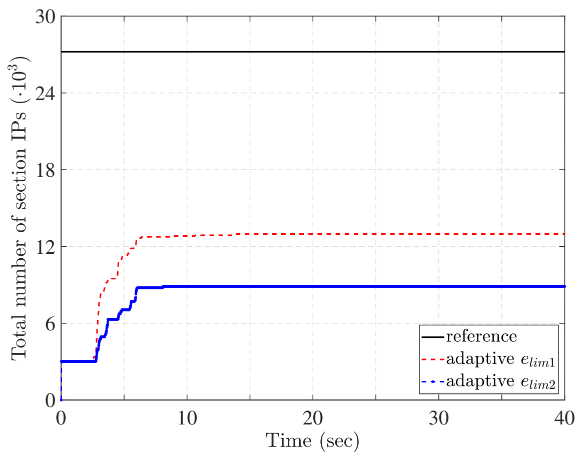

Fig. 14. Evolution of the total number of section integration points (IPs) under the Kobe acceleration record for the non-adaptive section discretization with 108 MP and for two adaptive schemes with strain limits $e_{lim,1}$ and $e_{lim,2}$.

In conclusion, the adaptive discretization reduces the computation time for the response history analysis by reducing the number of section integration points. Fig. 14 shows the evolution of the total number of section integration points during the dynamic response history analysis of the 6-story steel frame under the Kobe ground acceleration. For this model with 63 elements, 4 sections per element and 108 IPs per section, there is a total of 27216 material IPs for the non-adaptive discretization. The adaptive solutions start the analysis with 12 IPs per section for a total of 3024. The number of IPs increases during the analysis as inelastic strains appear at different sections of the structural model, activating them fully or partially. With a trigger strain value equal to the yield strain for the adaptive scheme $e_{lim,1}$, the total number of IPs at the end of the analysis is 12976, a little less than half of the number for the reference solution. For the Kobe ground acceleration these IPs come into play over a short time span between 3 and 6 sec in Figure 14, because of the strong acceleration pulse in the record. The computational savings relative to the reference solution amount to 50%, as Table 3 confirms. For the adaptive scheme $e_{lim,2}$ with a trigger strain value of twice the yield strain the total number of IPs at the end of the response history analysis is 8880 in Figure 14, about a third of the number for the reference solution. This reduces the analysis time to about 40% of the time required for the reference solution in Table 3. The significantly reduced number of material IPs in the structural model reduces the requirements for data storage and for post-processing the results of the response history analysis, which are not included in Table 3. The benefits can, therefore, be even more significant.

Table 3 shows that the reduction in analysis time is smallest for the Kobe acceleration record, because of the activation of all inelastic material IPs early in the response time history, as Figure 14 shows. For the other records in Table 3, the percentage of inelastic material IPs over the course of the response history analysis is smaller and the computational savings bigger.

Figs. 15-22 show the relative roof drift history at point A and the axial force-bending moment history at the base of column 1 for the structural model in Fig. 13. Figs. 15-18 show the response histories under the Kobe ground acceleration, which causes the largest inelastic deformations in the model, and consequently activates the largest number of inelastic material IPs. Figs. 19-22 show the same response histories under the Darfield, NZ ground acceleration. This record generates the largest relative error between the adaptive discretization schemes and the reference solution among all acceleration histories in Table 3.

The results in Figs. 15-22 demonstrate that the accuracy of the proposed adaptive section discretization schemes is excellent for the global displacements and the local forces. Very small errors appear in the history of local deformation measures when the trigger strain value of twice the yield strain is selected, but these are practically insignificant.

Further analyses of the 6-story frame under the Kobe and Landers earthquake motions were

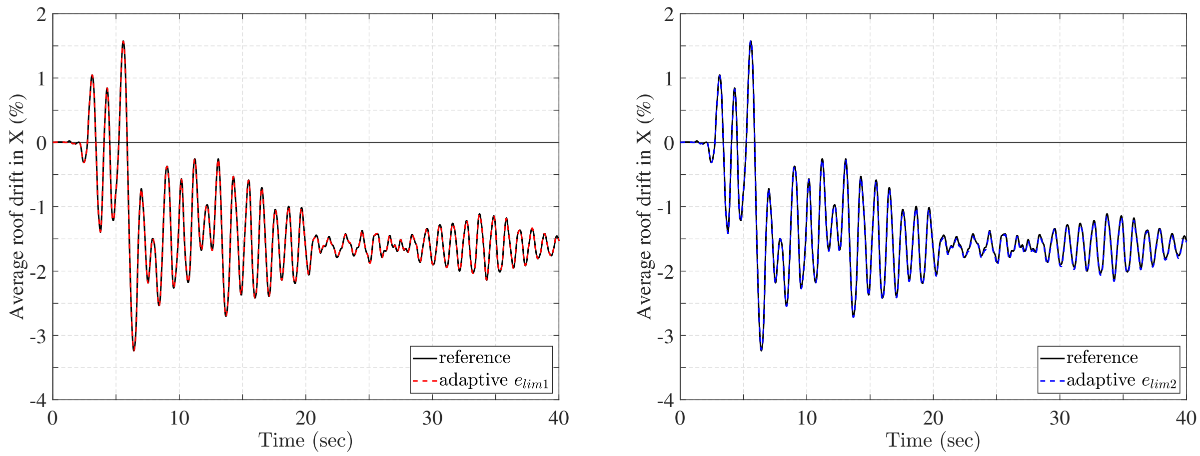

(a) (b)

Fig. 15. Relative roof drift in X under the Kobe ground acceleration for the non-adaptive section discretization with 108 MP and for two adaptive schemes with strain limits $e_{lim,1}$ and $e_{lim,2}$.

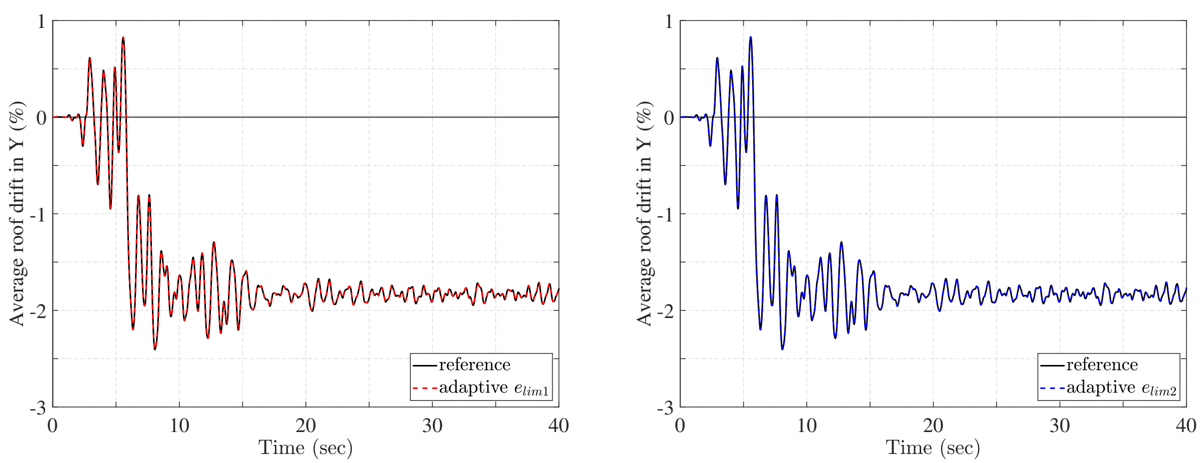

(a) (b)

Fig. 16. Relative roof drift in Y under the Kobe ground acceleration for the non-adaptive section discretization with 108 MP and for two adaptive schemes with strain limits $e_{lim,1}$ and $e_{lim,2}$.

undertaken with a non-adaptive section discretization for the girders with the smallest possible number of 12 IPs (Kostic and Filippou 2012), to take advantage of the fact that the girders are subjected to uniaxial bending on account of the in-plane rigidity of the floor diaphragm. For the columns the same three section discretizations as for the preceding analyses were studied: (1) a non-adaptive fiber mesh with 108 IPs, an adaptive scheme with a 3x12 fiber mesh for each activated flange and web for trigger strain values $e_{lim,1}$, and an adaptive scheme with a 3x12 fiber mesh

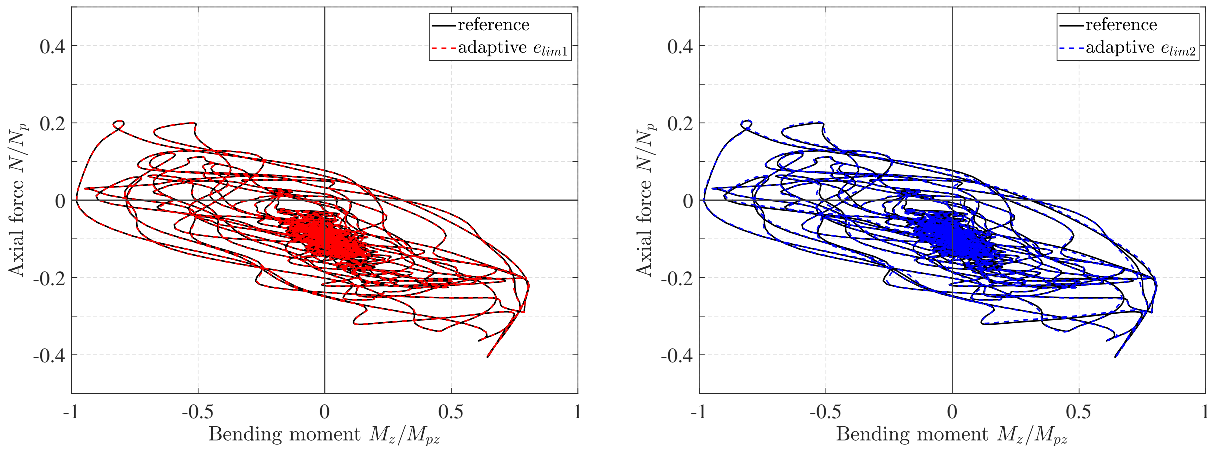

(a) (b)

Fig. 17. Normalized axial force N-bending moment M_z history at the base of column 1 under the Kobe ground acceleration for the non-adaptive section discretization with 108 MP and for two adaptive schemes with strain limits $e_{lim,1}$ and $e_{lim,2}$

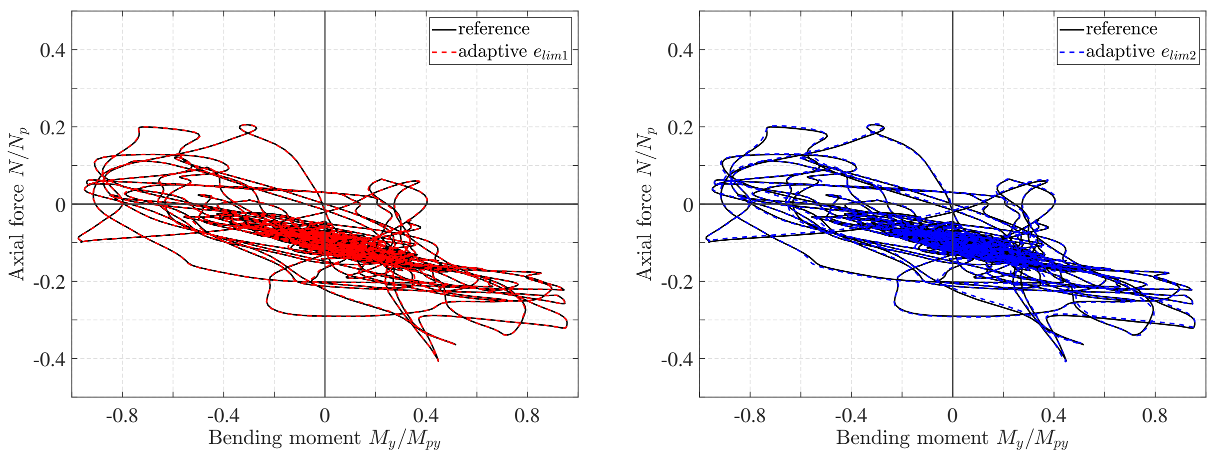

(a) (b)

Fig. 18. Normalized axial force N-bending moment M_y history at the base of column 1 under the Kobe ground acceleration for the non-adaptive section discretization with 108 MP and for two adaptive schemes with strain limits $e_{lim,1}$ and $e_{lim,2}$.

for each activated flange and web for trigger strain values $e_{lim,2}$. These studies confirmed the conclusions of this section, namely that

- either trigger strain criterion of $e_{lim,1}$ or $e_{lim,2}$ gives results of comparable accuracy with those in Figs. 15-22 for the global and the local response;

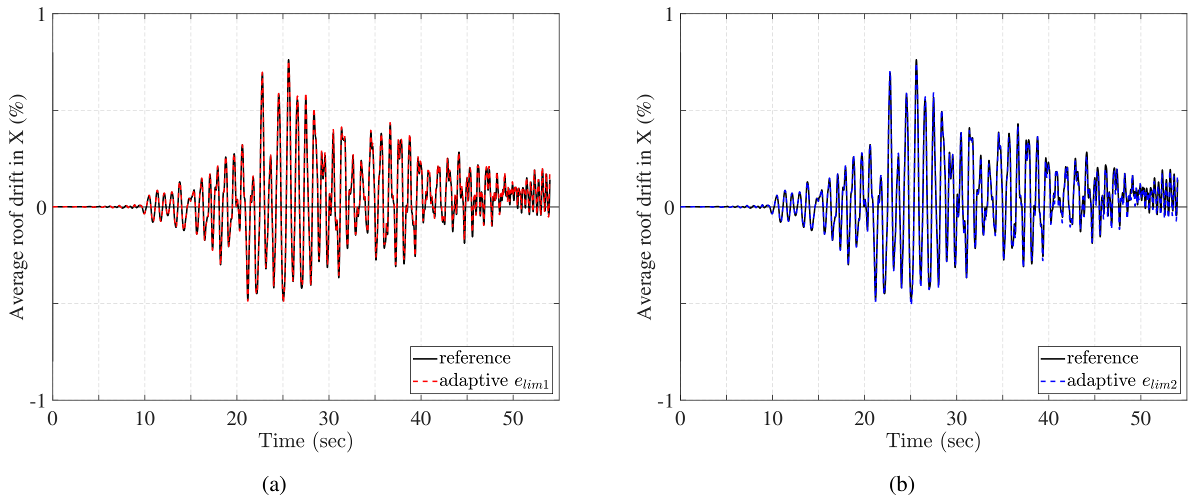

Fig. 19. Relative roof drift in X under the Darfield ground acceleration for the non-adaptive section discretization with 108 MP and for two adaptive schemes with strain limits $e_{lim,1}$ and $e_{lim,2}$.

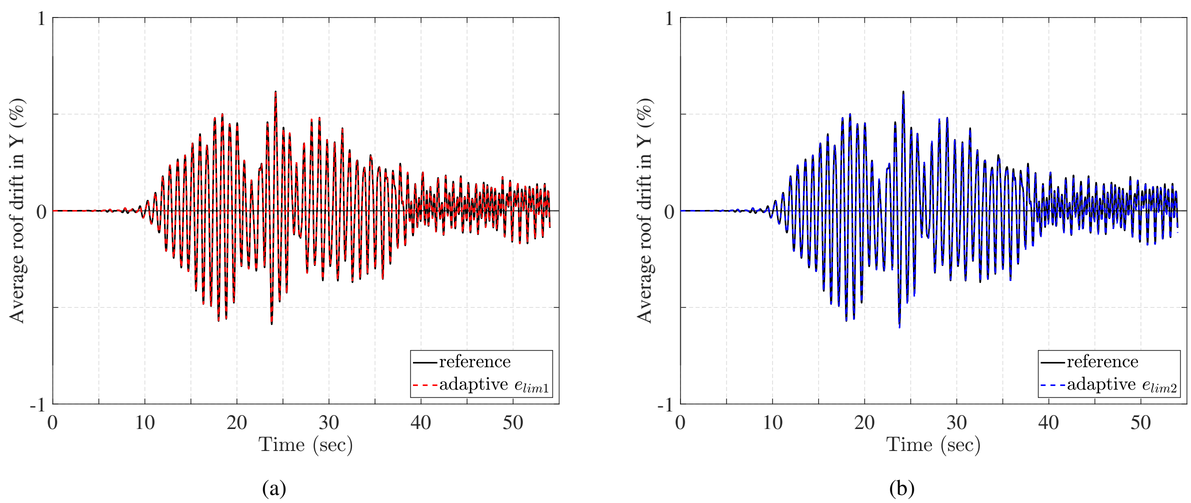

Fig. 20. Relative roof drift in Y under the Darfield ground acceleration for the non-adaptive section discretization with 108 MP and for two adaptive schemes with strain limits $e_{lim,1}$ and $e_{lim,2}$.

- the computational savings from the relaxation of the trigger strain criterion from the yield strain ($e_{lim,1}$) to twice the yield strain ($e_{lim,2}$) are so small as to not be significant.
- the computational effort for the adaptive scheme is 2 to 3 times smaller than for the non-adaptive scheme, even when it is applied only to the columns of the structural model.

It is, therefore, safe to conclude that the proposed adaptive section discretization scheme will offer significant computational savings for large structural models, even when it is applied only to those

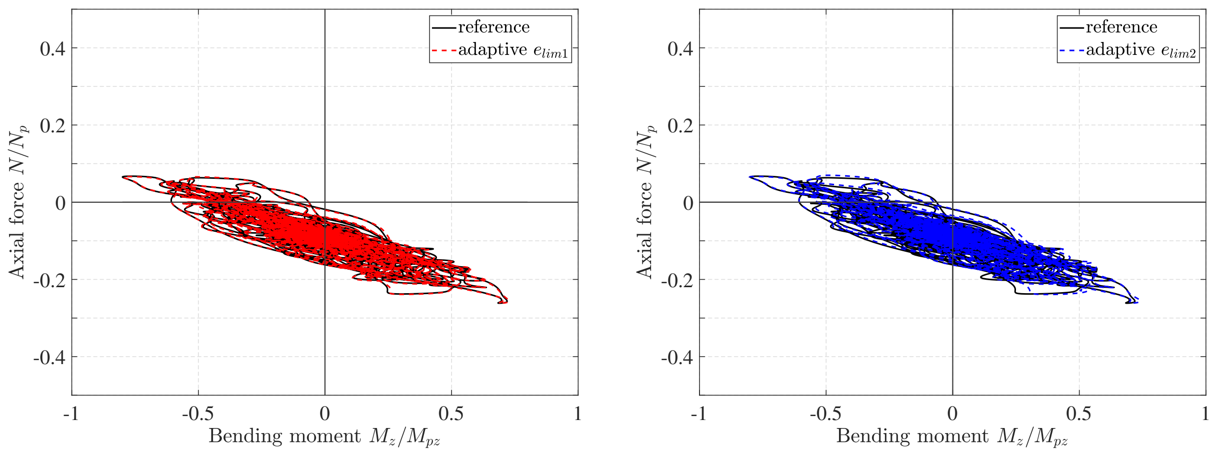

(a) (b)

Fig. 21. Normalized axial force N-bending moment M_z history at the base of column 1 under the Darfield ground acceleration for the non-adaptive section discretization with 108 MP and for two adaptive schemes with strain limits $e_{lim,1}$ and $e_{lim,2}$.

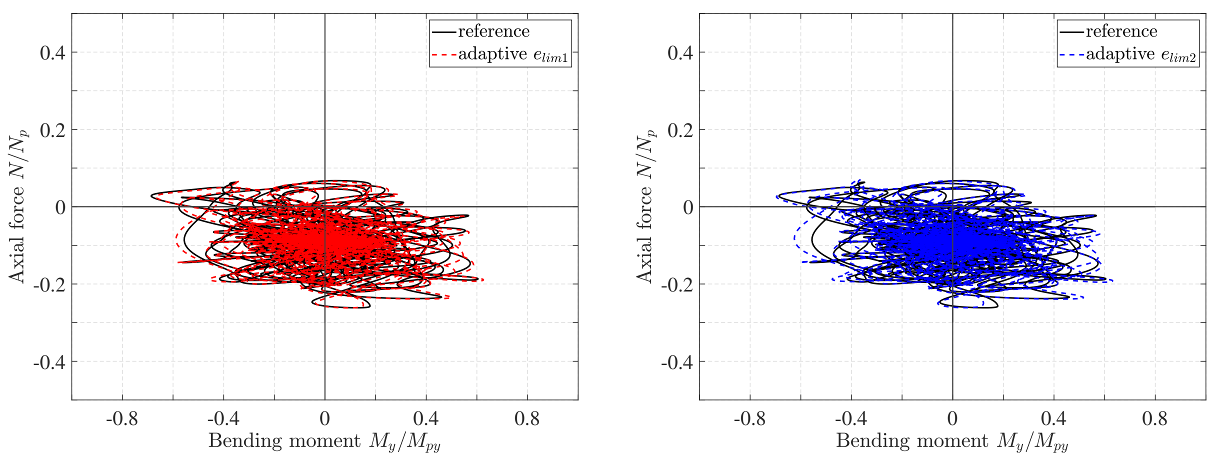

(a) (b)

Fig. 22. Normalized axial force N-bending moment M_y history at the base of column 1 under the Darfield ground acceleration for the non-adaptive section discretization with 108 MP and for two adaptive schemes with strain limits $e_{lim,1}$ and $e_{lim,2}$.

sections and elements that may experience inelastic deformations under uniaxial, but especially under biaxial flexure conditions.

CONCLUSIONS

The paper presents an adaptive section discretization scheme for the inelastic response analysis of structural members with cross sections that can be decomposed into rectangular and circular subdomains. Each subdomain can consist of a different material. As long as the largest strain in a subdomain does not exceed the specified trigger strain values, the subdomain contribution to the section response is determined by the numerically exact cubature rule for the subdomain. Once the largest strain reaches the trigger value for a subdomain, it is discretized with a fiber mesh and the numerical evaluation of its contribution to the section response is determined with the midpoint integration rule. The fiber mesh remains in effect for the activated subdomain until the end of the response history. The proposed adaptive discretization scheme is simple to implement in any nonlinear frame element that uses section integration for the evaluation of the inelastic response. Because the integration transition from the elastic to the inelastic range is gradual, the resulting response is smooth, thus ensuring numerical robustness.

The paper applies the proposed method to thin-walled sections composed of rectangular subdomains and investigates the effect of different trigger strain values on the accuracy and computational efficiency of the inelastic response analysis of wide-flange steel sections and multi-story steel frames under static and dynamic excitations.

For the studies in this paper the reference solution consists of a 3x12 fiber mesh for the flanges and the web for all sections of the beam-column elements in the structural model. The adaptive section discretization uses the same 3x12 fiber mesh for each rectangular subdomain so that the response of a wide-flange section with activation of both flanges and the web is practically indistinguishable from the reference solution. The adaptive section discretization maintains excellent accuracy for the global and local response measures of steel frames even for a trigger value of twice the yield strain for the activation of each subdomain. At the same time it takes advantage of the limited number of sections and section subdomains undergoing inelastic deformations during the response history to reduce the number of inelastic material stress-strain relations that need to be evaluated in a given load step. The resulting computational savings in the analysis time, the amount of data storage, and the time for post-processing are rather significant. Even for the structural models of this paper with a very modest number of elements to be monitored for inelastic action, the reduction in computation time ranges from 2.6 to 5 times relative to the non-adaptive reference solution.

These savings are expected to increase in proportion with the number of sections and elements that need to be monitored for inelastic action in a large structural model. The selection of either the yield strain or twice the yield strain as the trigger criterion for the activation of each subdomain has a relatively small effect on the computation time. This leads to the recommendation to use the yield strain as the trigger criterion ensuring the same accuracy for the global and the local response as the non-adaptive section discretization with the same number of IPs for each subdomain.

While the studies in this paper are limited to the fine mesh for the reference solution, as recommended by Kostic and Filippou (2012), similar results are expected for the coarser fiber mesh recommendation with 2x8 IPs in the flanges and 8x1 IPs in the web, as long as the adaptive discretization uses the same fiber mesh for the activated subdomains. The reason for this is that the ratio of activated subdomains is not expected to change. However, with the cubature rule for a rectangular subdomain requiring 4 IPs, the savings in material stress-strain evaluations for each inactive subdomain are smaller than for the fine mesh: 4 instead of 16 for the flange, and 4 instead of 8 for the web rather than 4 instead of 32 for each flange and web with the fine mesh. Because this coarse discretization leads to inaccuracies in local response measures, especially under biaxial flexure, Kostic and Filippou (2012) recommend that the fine mesh be used, unless the local response accuracy is carefully assessed with a preliminary study.

While space limitations did not allow for an exhaustive evaluation of the different options for the fiber mesh of the adaptive section discretization, it is promising that the proposed scheme permits customizing the computational time requirements of the structural model under specific accuracy requirements for the global and local inelastic response. The computational savings promise to be very significant, especially for large structural models with many sections to monitor for inelastic action under a suite of ground motions, as is commonly the case for performance-based analysis in regions of high seismic risk.

DATA AVAILABILITY STATEMENT

Some or all data, models, or code that support the findings of this study are available from the corresponding author upon reasonable request.

ACKNOWLEDGMENTS

The first author thanks Ministry of Science of the Republic of Serbia for financial support under the project number 2000092.

REFERENCES

Abramowitz, M., Stegun, I. A., and Miller, D. (1964). *Handbook of mathematical functions with formulas, graphs and mathematical tables (National Bureau of Standards Applied Mathematics Series No. 55)*. United States Department of Commerce, National Bureau of Standards.

Berry, M. P. and Eberhard, M. O. (2008). "Performance modeling strategies for modern reinforced concrete bridge columns." *Report no.*, PEER Report 2007/07, Department of Civil and Environmental Engineering, University of California, Berkeley, CA.

Cheng, J. and Shing, P. B. (2022). "Practical nonlinear analysis methods for flexure-dominated reinforced masonry shear walls." *Journal of Structural Engineering*, 148(8), 04022109.

Chiorean, C. (2009). "A computer method for nonlinear inelastic analysis of 3d semi-rigid steel frameworks." *Engineering Structures*, 31(12), 3016–3033.

Cools, R. (2003). "An encyclopaedia of cubature formulas." *Journal of Complexity*, 19(3), 445–453.

Crisfield, M. A. (1996). *NonLinear Finite Element Analysis of Solids and Structures, Volume 1*. John Wiley & Sons.

Filippou, F. C. and Constantinides, M. (2004). "Fedeaslab getting started guide and simulation examples." *Report No. NEESgrid-2004-22*, University of California, Berkeley.

Hajjar, J. F., Molodan, A., and Schiller, P. H. (1998). "A distributed plasticity model for cyclic analysis of concrete-filled steel tube beam-columns and composite frames." *Engineering Structures*, 20(4), 398–412.

He, Z., Fu, S., and Ou, J. (2017a). "State transformation procedures for fiber beam-column element in inelastic dynamic time history analysis for moment-resisting frames." *Journal of Computing in Civil Engineering*, 31(5), 04017036.

He, Z., Fu, S., Shi, Y., Tao, Q., and Sun, C. (2017b). "New speedup algorithms for nonlinear dynamic time history analysis of supertall building structures under strong earthquakes." *The Structural Design of Tall and Special Buildings*, 26(16), e1369.

Kostic, S. and Filippou, F. (2012). "Section discretization of fiber beam-column elements for cyclic inelastic response." *Journal of Structural Engineering*, 138(5), 592–601.

Kostic, S. and Filippou, F. (2022). "An adaptive fiber section discretization scheme for nonlinear frame analysis." *Journal of Structural Engineering*, Forthcoming.

Minafò, G. and Camarda, G. (2021). "Use of fiber-section beam elements for modelling the monotonic flexural response of rc jacketed columns." *Engineering Structures*, 228, 111503.

Neuenhofer, A. and Filippou, F. C. (1997). "Evaluation of nonlinear frame finite-element models." *Journal of Structural Engineering*, 123(7), 958–966.

Ngo-Huu, C., Kim, S.-E., and Oh, J.-R. (2007). "Nonlinear analysis of space steel frames using fiber plastic hinge concept." *Engineering Structures*, 29(4), 649–657.

Orbison, J. G., McGuire, W., and Abel, J. F. (1982). "Yield surface applications in nonlinear steel frame analysis." *Computer Methods in Applied Mechanics and Engineering*, 33(1), 557–573.

Quagliaroli, M., Malerba, P., and Sgambi, L. (2015). "A parametric subdomain discretization for the analysis of the multiaxial response of reinforced concrete sections." *Advances in Engineering Software*, 82, 87–104.

Scott, M. H., Fenves, G. L., McKenna, F., and Filippou, F. C. (2008). "Software patterns for nonlinear beam-column models." *Journal of Structural Engineering*, 134(4), 562–571.

Simo, J. C. and Hughes, T. J. (1998). *Computational Inelasticity*. Springer-Verlag New York, Incorporated, Secaucus, NJ, USA.

Taucer, F., Spacone, E., and Filippou, F. (1991). "A fiber beam-column element for seismic analysis of reinforced concrete structures." *Report UCB/EERC-91/17*, Earthquake Engineering Research Center, University of California, Berkeley.

Terzic, V. and Stojadinovic, B. (2015). "Evaluation of post-earthquake axial load capacity of circular bridge columns." *ACI Structural Journal*, 112(1), 23–33.